Viewpoint Paper

On plastic strain recovery in freestanding nanocrystalline metal thin films

Jagannathan Rajagopalan,* Jong H. Han and M. Taher A. Saif

Department of Mechanical Science and Engineering, University of Illinois at Urbana-Champaign, Urbana, IL 61801, USA

Abstract—In a recent article [J. Rajagopalan, J.H. Han, M.T.A. Saif, Science 315 (2007) 1831–1834], we have reported substantial (50–100%) plastic strain recovery in freestanding nanocrystalline metal films (grain size 50–65 nm) after unloading. The strain recovery was time dependent and thermally activated. Here we model the time evolution of this strain recovery in terms of a thermally activated dislocation propagation mechanism. The model predicts an activation volume of $\approx 42b^3$ for the strain recovery process in aluminum.
© 2008 Acta Materialia Inc. Published by Elsevier Ltd. All rights reserved.

In coarse-grained polycrystalline metals, plastic deformation proceeds through the propagation of dislocations generated by intragranular dislocation sources. During their propagation, these dislocations interact with pre-existing features such as grain boundaries as well as each other, in the process being annihilated or forming new dislocations [1]. These interactions determine the onset of macroscopic yielding and the subsequent strain hardening, and in effect control the plastic behavior of these metals [2].

In nanocrystalline metals, where the grain size is typically less than 100 nm, intragranular dislocation sources such as the Frank–Read source cease to operate [3,4] since the stress needed to bow out the dislocation becomes very large [5]. This lack of conventional dislocation sources in nanocrystalline metals results in high strength, often an order of magnitude larger than coarse-grained metals, and limited ductility [6,7]. The inability of nanocrystalline metals to deform by conventional means results in unusual deformation mechanisms. Molecular dynamics (MD) simulations [8–10] suggest that plastic deformation in nanocrystalline metals is carried out by dislocations nucleated at the grain boundaries; once nucleated, these dislocations travel across the grains and eventually get absorbed in the opposite grain boundary. MD simulations and some experiments further suggest that at very small grain sizes (≈ 10 nm), grain boundary sliding and migration become increasingly important and cause a reduction in strength [11–14].

However, irrespective of the grain size or the deformation mechanisms involved, plastic deformation is considered irrecoverable. In a recent article [15], we have shown that freestanding aluminum and gold nanocrystalline thin films, with an average grain size of 65 and 50 nm, respectively, recover a substantial fraction (50–100%) of plastic deformation after unloading, i.e. under a macroscopically stress-free condition. This strain recovery was time dependent and thermally activated. Both the aluminum and gold films were 200 nm thick and were deformed under uniaxial tension. Here, we first discuss the deformation behavior of these films in the context of this unexpected strain recovery. We then interpret and model the time evolution of strain recovery in terms of a thermally activated dislocation propagation mechanism suggested by MD simulations [16].

We begin by summarizing the main observations reported in Ref. [15].

1. Nanocrystalline aluminum and gold thin film specimens (grain size 50–65 nm) recover a substantial fraction of plastic deformation after unloading.
2. After strain recovery, the specimens show no residual hardening during the next loading, i.e. the stress–strain behavior is almost unchanged (Fig. 1a).

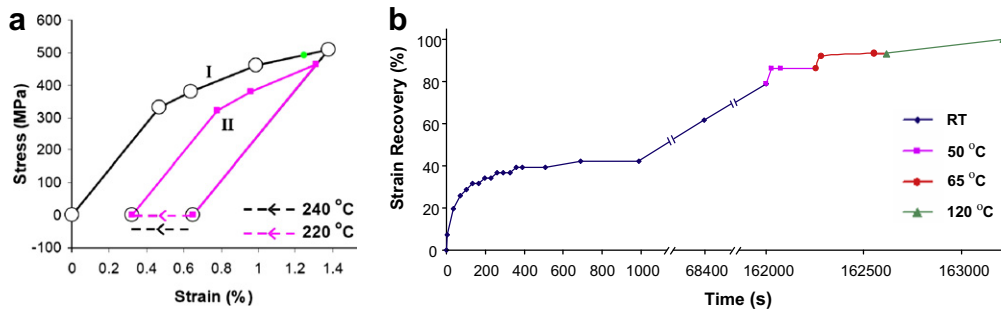* Corresponding author. Tel.: +1 217 244 2760; e-mail: jrajago2@uiuc.edu

Figure 1. (a) Stress–strain curves for an aluminum specimen showing plastic strain recovery and the absence of residual hardening during the next loading [15]. The dashed arrows indicate strain recovery at different annealing temperatures. (b) Time evolution of strain recovery at different annealing temperatures in an aluminum specimen [15]. About 40% of strain recovery at room temperature (RT) happens within 400 s, whereas the rest of the recovery takes much longer time. The spurts in recovery after increasing the temperature saturate in a short period of time. This specimen was deformed to ≈1.25% strain (green dot in (a)) during loading. (For interpretation of the references to colour in this figure legend, the reader is referred to the web version of this article.)

3. The strain recovery occurs under a macroscopically stress-free condition and is time dependent and thermally activated (Fig. 1b).

First, we consider the large strain hardening exhibited by the films (Fig. 1a) immediately after yielding during loading. In coarse-grained face-centered cubic metals, strain hardening occurs due to formation of permanent dislocation networks. Dislocations, generated by Frank–Read sources, that propagate in intersecting slip planes interact and form immobile dislocations, which obstruct the propagation of other dislocations and hence harden the crystal. But such a mechanism cannot be responsible for the strain hardening observed in these films because of the paucity of intragranular dislocation sources in nanocrystalline metals. However, this apparent strain hardening can be understood as the consequence of inhomogeneous deformation as explained below.

During the initial stages of deformation, all grains deform elastically. After the macroscopic yield point is reached, dislocation activity (e.g. dislocation nucleation from grain boundaries) starts in relatively larger grains with favorable local stress conditions/grain boundary orientations, whereas smaller or unfavorably oriented grains accommodate the strain elastically. This inhomogeneous deformation leads to a reduced stress–strain slope and manifests as apparent strain hardening. Furthermore, the stress distribution becomes nonuniform with lower stresses in larger grains and higher stresses in smaller grains, which results in residual internal stresses upon unloading. These internal stresses provide the driving force for reverse plastic flow and hence strain recovery (Fig. 2). Note that because of the small grain size, intragranular dislocation sources are scarce and grain boundaries are likely to act as dislocation sources. As these dislocations nucleated at the grain boundaries propagate, they could be pinned by obstacles at the grain boundaries with further propagation through thermally activated depinning [16]. This process leads to the time and temperature dependence of strain recovery.

Next, we consider the lack of residual hardening in the films after strain recovery. Mobile dislocations in polycrystalline metals experience resistance due to forces arising from their long-range elastic interactions with
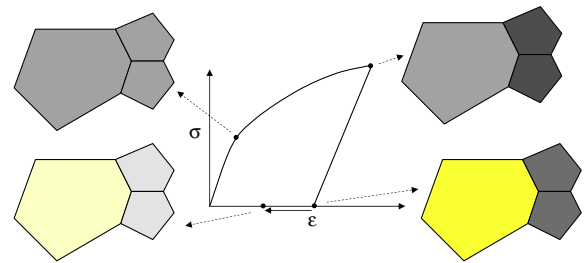

Figure 2. The stresses in a large and two surrounding smaller grains during loading and strain recovery. Grey and yellow colors indicate tensile and compressive stress and darker shades represent higher magnitude. At the end of loading, the large grain has lower stress as it has deformed plastically. As a result, the large grain is under compression whereas the smaller grains are under tension after unloading. Reverse plastic flow in the larger grain leads to strain recovery and a reduction in the internal stresses. (For interpretation of the references to colour in this figure legend, the reader is referred to the web version of this article.)

the substructure as well as short-range interactions with obstacles such as impurities, solute atoms, forest dislocations and grain boundary structures. In a simplified picture, the stress experienced by a dislocation due to its interactions with other dislocations and the grain boundaries can be denoted by an internal stress τ_i. The difference between the applied shear stress (τ) and τ_i is the effective shear stress, τ^*, acting on the dislocation [17]

$$\tau = \tau_i + \tau^* \qquad (1)$$

τ^* in combination with thermal fluctuations assists the dislocations to overcome local obstacles. Therefore, the effective shear stress required by dislocations to overcome local barriers is temperature dependent. τ_i, on the other hand, is athermal and depends only on strain. Suppose a critical effective shear stress (τ_c^*) is needed for dislocations to propagate at a given temperature, then the macroscopic stress (τ_y) corresponding to τ_c^* would be the yield stress.

When strain recovery is complete there are no residual stresses arising from deformation, and therefore the internal stresses acting on dislocations (τ_i) remains

unaltered. Hence, the applied stress required to propagate dislocations during the next loading remains unchanged, i.e. τ_y remains constant. On the other hand, if strain recovery is incomplete, the grains that have undergone large plastic deformation still experience the residual stress fields arising from the elastically deformed neighboring grains. Because of these residual stresses a larger applied stress is required to reach τ_c^* during the next loading, resulting in an increase in τ_y [15].

In the above discussion it is assumed that there are no major changes in the substructure during deformation that would substantially alter the internal stress fields. The rationale for such an assumption is as follows. As mentioned earlier, MD simulations show that during plastic deformation of nanocrystalline metals dislocations nucleate at the grain boundaries, travel across the grains and get absorbed in the opposite grain boundaries without forming any permanent dislocation networks. These simulation results are consistent with experiments [18,19], which have revealed that X-ray peak broadening during deformation of nanocrystalline nickel is completely reversible upon unloading, i.e. no residual dislocation network is accumulated during deformation.

We now consider the time evolution of strain recovery. As mentioned earlier, MD simulations have shown that dislocation propagation in nanocrystalline metals is hindered by grain boundary structures such as ledges that act as pinning points and that further propagation takes place through thermally assisted depinning. This picture of dislocation propagation has been found to be consistent with stress reduction experiments [20] and activation volume measurements [21,22] on nanocrystalline nickel. Therefore, it is reasonable to assume that such a process is active in our samples, where apart from grain boundary structures, impurity clusters at boundaries could also hinder dislocation propagation. For simplicity, we assume that there are just two types of obstacles (Fig. 3), which require activation energies E_{a1} and $E_{a2}(>E_{a1})$, respectively, to be overcome. Since the strain recovery is a thermally activated process, the strain recovery rate when passing over obstacles of types I and II can be expressed as

Figure 3. Two dislocations pinned by two different sets of obstacles during strain recovery. The force for the reverse glide of the dislocations arises from the residual stresses that result from inhomogeneous deformation.

$$\dot{\gamma}_i = \dot{\gamma}_{0i}\exp((-E_{ai} + \tau^* v_i)/kT) \quad i = 1, 2 \tag{2}$$

Here, $\dot{\gamma}_{0i}$ are constants, v_i are activation volumes, k is the Boltzmann constant and T is the temperature. During strain recovery, since τ is zero (the specimens are macroscopically stress free), $\tau^* = -\tau_i$ from Eq. (1). The residual stress fields that contribute to τ_i decrease with strain recovery. Hence the recovery rate also decreases with strain recovery. However, at any point in time during strain recovery there are large number of dislocations that are passing though both types of obstacles and hence the macroscopic recovery rate

$$\dot{\gamma} = \alpha(\gamma)\dot{\gamma}_1 + \beta(\gamma)\dot{\gamma}_2 \tag{3}$$

Here, α and β are the fractions of dislocations pinned by type I and type II obstacles, respectively. Note that α and β change with γ as explained below.

Since $E_{a2} > E_{a1}$ the dislocations pinned by type II obstacles take much more time to depin compared to those pinned by type I obstacles. If $t_1 = 1/\dot{\gamma}_1$ and $t_2 = 1/\dot{\gamma}_2$, dislocations pinned by type II obstacles remain stationary at time scales of the order of t_1. Hence, at the initial stages of strain recovery $\dot{\gamma}$ is proportional to $\dot{\gamma}_1$. However, as strain recovery progresses, even dislocations that are initially pinned by type I obstacles start encountering type II obstacles as they propagate and become stationary. Hence, β increases as strain recovery increases. When β approaches 1, the strain recovery rate approaches $\dot{\gamma}_2$ and remains proportional to it until the end of the recovery. The strain recovery can hence be classified into two distinct regimes, where the recovery rate is characterized by $\dot{\gamma}_1$ and $\dot{\gamma}_2$, respectively.

If γ_{rt} is the total recoverable strain, we can obtain an estimate of the crossover strain, γ_{rc}, at which the strain recovery rate becomes proportional to $\dot{\gamma}_2$, as follows. Suppose there are, on average, n obstacles per unit length of the grain boundary in a material with grain size d. The dislocations encounter $nd = N$ obstacles as they travel across the grains, of which we assume N_1 to be type I obstacles and N_2 to be type II obstacles $(N_1 + N_2 = N)$. Further, we assume these obstacles to be randomly distributed and equally spaced, so that the strain (recovery) increment for each successful jump across an obstacle is the same. When all the dislocations cross these N obstacles, we get complete recovery.

The strain recovery rate becomes proportional to $\dot{\gamma}_2$ when all the dislocations get pinned by type II obstacles. However, each dislocation can encounter its first type II obstacle at a different stage. If N_{IA} is the average number of type I obstacles encountered by the dislocations before a type II obstacle, the ratio N_{IA}/N provides a measure of γ_{rc}/γ_{rt}. N_{IA} is given by

$$N_{IA} = \sum_{i=1}^{N_1} iP(i) \tag{4}$$

Here, $P(i)$ is the probability of encountering exactly i type I obstacles before a type II obstacle. $P(i)$ can be calculated as follows. Since there are totally N obstacles and N_1 are type I obstacles, the probability of the first obstacle being type I is N_1/N. The probability of the second obstacle being type I, given that the first obstacle is type I is $(N_1 - 1)/(N - 1)$. Therefore, the probability of
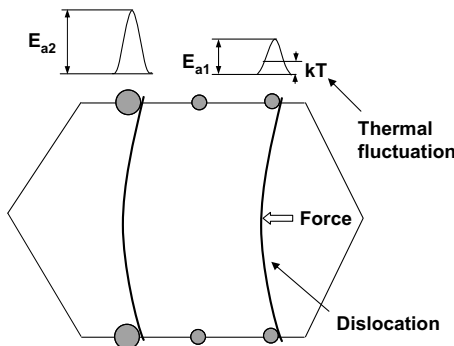
encountering two consecutive type I obstacles is $\frac{N_1}{N}\frac{N_1-1}{N-1}$. The probability of encountering exactly two type I obstacles before a type II obstacle is $\frac{N_1}{N}\frac{N_1-1}{N-1}\frac{N_2}{N-2}$. The third term is the probability that the third obstacle is of type II. Extending this, we get

$$P(i) = \frac{N_1}{N}\frac{N_1-1}{N-1}\frac{N_1-2}{N-2}\cdots\frac{N_1-i+1}{N-i+1}\frac{N_2}{N-i} \quad (5)$$

Beyond γ_{rc}, the dislocations still encounter type I obstacles, but the recovery rate is controlled by type II obstacles. This is because the time required to cross type II obstacles ($\propto t_2$) is much larger than that for type I obstacles ($\propto t_1$). In other words, dislocation jumps across type II obstacles is the rate-limiting process. The above analysis can be extended to scenarios where there are more than two types of obstacles, in which case there will be corresponding number of stages in strain recovery, the later stages characterized by increasingly larger activation energies. It is also worth noting that N_{IA}/N (Eqs. (4) and (5)) decreases with increasing N even when the proportion of type I and type II obstacles, i.e. $N_1:N_2$, remains constant (Fig. 4). Therefore γ_{rc}/γ_{rt}, i.e. the fraction of strain that recovers quickly, decreases with increasing N. Hence, if two specimens have the same distribution and density (n) of pinning points, the specimen with a smaller grain size, and hence a smaller N ($=nd$), will show a more pronounced recovery immediately after unloading.

This analysis provides a possible explanation for the time evolution of strain recovery shown in Figure 1b. The initial fast recovery ($\approx 40\%$ of total recovery) at room temperature (RT) is due to the passage of dislocations over low activation barriers. This phase of strain recovery terminates quickly as the dislocations start encountering larger barriers, and the following phase of RT recovery takes much longer. When temperature is increased to 50 °C, the dislocations overcome larger energy barriers more quickly and hence there is a sharp spurt in recovery. This spurt in recovery saturates in a short period of time because the temperature increase is not sufficient to overcome certain barriers, at least within the experimental timescales. The same characteristics are observed for annealing at 65 °C, with full recovery obtained at 120 °C. In this context, it is worth
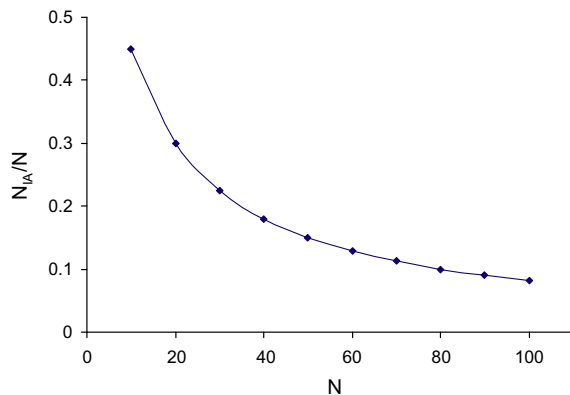
noting that Auger electron spectroscopy [15] revealed the presence of three impurities (oxygen, nitrogen and carbon) in the aluminum films. The spurts in the recovery rate at 50, 65 and 120 °C could be related to these three impurities. However, since the form (interstitial, substitutional or precipitate), spatial distribution and local concentrations of these impurities are unknown, a direct correlation is not possible.

Note that even if strain recovery is governed by a single activation energy, the recovery rate will decrease with increasing strain recovery since the effective stress τ^* acting on the dislocations will also reduce. However, a single activation barrier cannot account for the spurts and subsequent saturation of strain recovery on increasing the temperature, or the rapid fall in recovery rate at the early stages of recovery.

We now use the model described above to interpret the experimental data in Figure 1b and extract some physically relevant parameters governing the strain recovery. Note that in Figure 1b the recovered strain is normalized with respect to the total recoverable strain and in all our calculations below we use this normalized strain. We denote this normalized recovered strain as γ_r.

Since the initial phase of fast recovery at room temperature saturates at 42% (Fig. 1b), $\gamma_{rc} = 0.42$. Hence, until this point the recovery can be assumed to be governed by a single activation energy and activation volume. Therefore, combining with Eq. (2), Eq. (3) reduces to

$$\dot{\gamma}_r = \alpha(\gamma_r)\,\dot{\gamma}_0\exp((-E_a + \tau^*v)/kT) \quad \gamma_r \leqslant \gamma_{rc} = 0.42 \quad (6)$$

As the strain recovery proceeds, the residual stresses reduce and so does τ^*. Because this reduction is directly proportional to the strain recovered and the residual stresses vanish upon full recovery $\tau^* = \tau_0^*(1 - \gamma_r)$, where τ_0^* is the effective shear stress acting on the dislocations at the beginning of strain recovery. Similarly α also reduces with γ_r as progressively more dislocations get pinned by larger obstacles, with $\alpha \to 0$ at $\gamma = \gamma_{rc}$. To determine how α varies with γ_r one needs to know the exact density and distribution of the obstacles. Since this is unknown, we assume, for simplicity, $\alpha = \alpha_0(1 - \gamma_r/\gamma_{rc})$. Using these relations and noting that $\dot{\gamma}_0$, E_a, v, and T are constants and $\gamma_{rc} = 0.42$, Eq. (6) can be simplified to

$$\dot{\gamma}_r = A\exp(B(1-\gamma_r))(1-\gamma_r/0.42) \quad \gamma_r \leqslant 0.42 \quad (7)$$

where $A = \alpha_0\dot{\gamma}_0\exp(-E_a/kT)$ and $B = \tau_0^*v/kT$ are unknown constants.

Eq. (7) provides the time evolution for the initial phase of strain recovery. Experimental data of γ_r as a function of time (Fig. 1b) can be used to extract the constants A and B. For example, we plot the experimental $\dot{\gamma}_r$ vs. γ_r (Fig. 5a) and use Eq. (7) to best fit the data by the least-squares technique. The values of A and B, thus estimated, are 3.97×10^{-5} s^{-1} and 6.153.

It is not possible to extract E_a from A since α_0 and $\dot{\gamma}_0$ are unknown. However, since k and T are known, one can obtain the activation volume v from B if τ_0^* is known. We estimate τ_0^* as follows. At unloading (green dot in Fig. 1a), $\sigma \approx 500$ MPa, $\epsilon \approx 1.25\%$ and σ–ϵ slope is ≈ 13 GPa. If we assume no strain hardening (ideal plasticity) in the plastically deforming grains, only the

Figure 4. Variation of N_{IA}/N, which provides a measure of strain that recovers quickly, where N is a constant ratio of type I to type II obstacles ($N_1:N_2 = 9:1$).

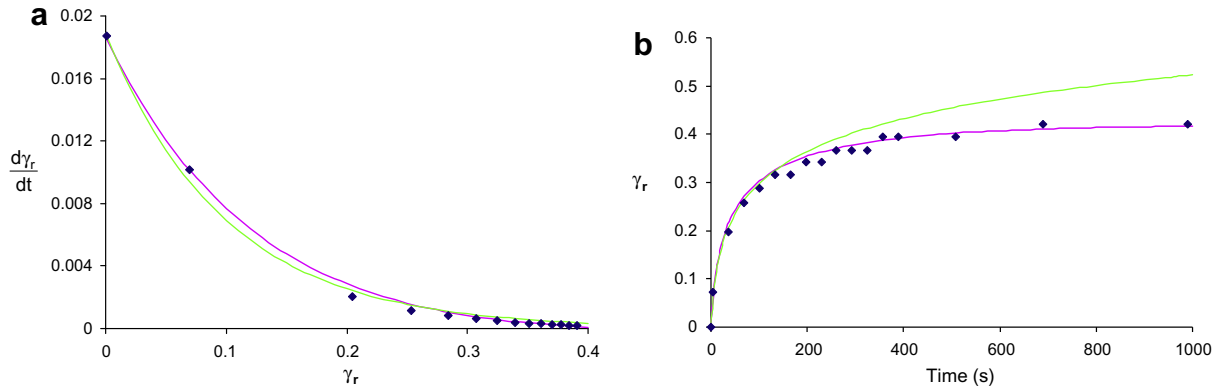**Figure 5.** (a) $\dot{\gamma}_r$ vs. γ_r data (blue diamonds) extracted from the experiments. Pink and green curves correspond to the best fits of Eqs. (7) and (9) to the extracted data, respectively. The $\dot{\gamma}_r$ vs. γ_r data corresponding to the first 400 s was used to fit both the curves. (b) Plot of γ_r vs. t obtained by numerically solving Eq. (7) (pink curve) and Eq. (9) (green curve). Note that when the variation of α with γ_r is ignored (Eq. (9)) the calculated values substantially exceed the measured values (blue diamonds) of γ_r. (For interpretation of the references to colour in this figure legend, the reader is referred to the web version of this article.)

elastically deforming grains, which have an elastic modulus of $\approx$70 GPa, would contribute to the stiffness of the film. The fractional area, x, of such elastically deforming grains on the cross-section of the specimen is thus 13/70 = 0.186. The average stress in the plastically deforming grains (σ_p) can be obtained by force balance:

$$x\epsilon E + (1-x)\sigma_p = \sigma \qquad (8)$$

σ_p is thus 415 MPa. Therefore, the average residual stress in these plastically deforming grains upon unloading will be 500–415 = 85 MPa. If one assumes a Schmid factor of 0.3, the residual resolved shear stress would be 25.5 MPa. Since the applied shear stress is zero, this would be the effective shear stress (Eq. (1)) acting on the dislocations in these grains. In other words $\tau_0^* = 25.5$ MPa. Using this value of τ_0^* and $T = 298$ K, we obtain from B an activation volume $v = 9.92 \times 10^{-28}$ m$^3 \approx 42b^3$. Here, $b = 0.286$ nm is the Burgers vector of aluminum. This activation volume of $42b^3$, we note, is fully consistent with other estimates of v for dislocation mediated plasticity in nanocrystalline metals [23,24].

Next, we use these estimated values of A and B to solve Eq. (7) numerically and obtain the time evolution of γ_r (Fig. 5b). The excellent agreement between the calculated and measured values of γ_r suggests that the model provides a realistic description of the strain recovery process. We note that even if we use only the first 300 s of the strain recovery data to obtain A and B, we still get a reasonably consistent value of v ($\approx 46b^3$) and good agreement between the calculated and measured values of γ_r. On the other hand, if we assume that the entire process is governed by a single activation energy, i.e. $\alpha = \alpha_0$ in Eq. (6), Eq. (7) takes the form

$$\dot{\gamma}_r = A^* \exp(B^*(1-\gamma_r)) \qquad (9)$$

If we use the experimentally obtained $\dot{\gamma}_r$ vs. γ_r data to estimate A^* and B^* (again using a least-squares fit) and use these values to solve Eq. (9) numerically, then the calculations substantially overestimate γ_r even at $t = 1000$ s (Fig. 5b). The difference between the calculated and measured values of γ_r becomes even more pronounced as t

increases. This suggests that the strain recovery cannot be described by a single activation energy.

In this work, we have analyzed the plastic strain recovery in nanocrystalline thin metal films. Specifically:

1. The deformation behavior of the these films, especially the apparent strain hardening during loading, has been interpreted in the context of strain recovery.
2. The lack of residual hardening in the films after complete strain recovery has been explained.
3. A semi-quantitative model based on thermally activated dislocation jumps over grain boundary obstacles has been proposed to qualitatively explain the time evolution of strain recovery.
4. Based on this model, the activation volume governing the strain recovery has been estimated.

The key underlying idea is that deformation and hence the stress distribution in these films could be highly inhomogeneous because of microstructural variations such as size and orientation of individual grains. This inhomogeneous deformation results in storage of elastic energy during deformation, which drives the strain recovery after unloading. While the arguments based on inhomogeneous deformation adequately explain the macroscopic deformation behavior and strain recovery, the microscopic mechanism that governs the deformation and strain recovery in not clear. The dislocation-based mechanism provides a reasonable explanation for the observed behavior but other mechanisms are possible as well.

In fact, a deformation model based on heterogeneous grain boundary diffusion and sliding [25] has been shown to result in strain recovery as well. In this model, during deformation the grain boundaries with higher diffusivities relax their stresses through diffusion, whereas low diffusivity boundaries do not. After unloading, the elastic energy stored in low diffusivity boundaries causes reverse diffusion in high diffusivity boundaries and hence strain recovery. While this model qualitatively predicts several aspects of the strain recovery, it deviates notably in some aspects. For example, in Ref. [25] the predicted stress–strain slope during the

initial phase of loading is substantially smaller compared to the unloading slope, in contrast to the observations in Ref. [15]. This difference in the loading and unloading slopes seems to arise because of the continuous stress relaxation in high diffusivity boundaries even at low stresses during loading, a direct result of assuming diffusion as the primary plastic deformation mechanism.

However, despite the differences in the assumed microscopic mechanism, the macroscopic phenomena underlying both the model presented here and in Ref. [25] is the same, namely the heterogeneity of the stress distribution. Deformation and annealing experiments in situ in a transmission electron microscope would be one way to obtain definitive information about the actual microscopic mechanism.

Finally, it is worth noting that there have been no previous reports of substantial strain recovery in coarse-grained metals even though there are inherent variations in the microstructure (e.g. a distribution of grain sizes) in these metals as well. This suggests that inhomogeneities in the microstructure become important only when the average grain size becomes sufficiently small. In other words, the strain recovery seems to result from the combined effect of a small mean grain size and the variations in the microstructure. Hence, to understand plasticity in nanocrystalline metals we might need to consider both the microstructural size as well as the variations in it.

Acknowledgements

References

[1] J.H. Hirth, J. Lothe, Theory of Dislocations, Wiley-Interscience, New York, 1982.
[2] A. Puskar, Microplasticity and Failure of Metallic Materials, Elsevier, Amsterdam, 1989.
[3] M. Legros, B.R. Elliot, M.N. Rittner, J.R. Weertman, K.J. Hemker, Philosophical Magazine A 80 (2000) 1017–1026.
[4] M.A. Haque, M.T.A. Saif, Journal of Materials Research 20 (2005) 1769–1777.
[5] G. Saada, Materials Science and Engineering A 400–401 (2005) 146–149.
[6] M. Haque, M.T.A. Saif, Scripta Materialia 47 (2002) 863–867.
[7] Y.M. Wang, K. Wang, D. Pan, K.J. Lu, K. Hemker, E. Ma, Scripta Materialia 48 (2003) 1581–1586.
[8] V. Yamakov, D. Wolf, S.R. Phillpot, A.K. Mukherjee, H. Gleiter, Nature Materials 3 (2004) 43–47.
[9] J. Schiotz, K.W. Jacobsen, Science 301 (2003) 1357–1359.
[10] H. Van Swygenhoven, P.M. Derlet, A. Hasnaoui, Physical Review B 66 (2002) 024101.
[11] J. Schiotz, F.D. Tolla, K.W. Jacobsen, Nature 391 (1998) 561–563.
[12] V. Yamakov, S.R. Wolf, D. Phillpot, A.K. Mukherjee, H. Gleiter, Nature Materials 1 (2002) 45–49.
[13] H. Conrad, J. Narayan, Applied Physics Letters 81 (2002) 2241–2243.
[14] K.J. Van Vliet, S. Tsikata, S. Suresh, Applied Physics Letters 83 (2003) 1441–1443.
[15] J. Rajagopalan, J.H. Han, M.T.A. Saif, Science 315 (2007) 1831–1834.
[16] H. Van Swygenhoven, P.M. Derlet, A. Froseth, Acta Materialia 54 (2006) 1975–1983.
[17] A. Seeger, J. Diehl, S. Mader, H. Rebstock, Philosophical Magazine 2 (1957) 323–350.
[18] Z. Budrovic, H. Van Swygenhoven, P.M. Derlet, S. Van Petegem, B. Schmitt, Science 304 (2004) 273–276.
[19] S. Brandstetter, Z. Budrovic, S.V. Petegem, B. Schmitt, E. Stergar, P.M. Derlet, H.V. Swygenhoven, Applied Physics Letters 87 (2005) 231910.
[20] S. Van Petegem, S. Brandstetter, H. Van Swygenhoven, J.-L. Martin, Applied Physics Letters 89 (2006) 073102.
[21] Y.M. Wang, A.V. Hamza, E. Ma, Applied Physics Letters 86 (2005) 241917.
[22] Y.M. Wang, A.V. Hamza, E. Ma, Acta Materialia 54 (2006) 2715–2726.
[23] L. Lu, R. Schwaiger, Z.W. Shan, M. Dao, K. Lu, S. Suresh, Acta Materialia 53 (2005) 2169–2179.
[24] Y.M. Wang, E. Ma, Material Science and Engineering A 375–377 (2004) 46–52.
[25] Y. Wei, A.F. Bower, H. Gao, Scripta Materialia 57 (2007) 933–936.